Direct-Coupled Plasma-Assisted Combustion Using a Microwave Waveguide Torch

Stephen Hammack, *Student Member, IEEE*, Xing Rao, Tonghun Lee, and Campbell Carter

***Abstract*—A tunable microwave waveguide is used to initiate and enhance combustion by coupling an atmospheric plasma discharge to a premixed methane/air flame. The absorbed microwave power ranges from 60 to 150 W, which was generated from a continuous source operating at 2.45 GHz, whereas combustion power ranges from 200 to 1000 W. OH radical number densities were measured using planar laser-induced fluorescence (PLIF), and temperatures were measured using Rayleigh scattering thermometry for various flow rates, equivalence ratios, and power levels. Increases in reaction volume, OH density, and temperature were observed as power increased. In the plasma-coupled premixed flame, OH number densities, which are quantified on the order of 10^{16} cm^{-3}, increased by up to 50%, and temperature ranging from 2000 to 3000 K increased by up to 40% as the absorbed microwave power was increased from 60 to 130 W. Air-only plasma discharges exhibited a much greater temperature increase, i.e., up to 190%. The power associated with the measured temperature increases varied greatly with flow and input power but are typically three to four times greater in the air-only plasma compared to the flame coupled plasma, demonstrating a greater degree of nonthermal mechanisms present in plasma-enhanced flame discharge.**

***Index Terms*—Energetically enhanced combustion, microwave plasma, planar laser-induced fluorescence (PLIF), plasma-assisted combustion (PAC), Rayleigh scattering thermometry.**

I. Introduction

ELECTROMAGNETICALLY enhanced oxidation holds great potential to be the foundation of an improved energy infrastructure by facilitating highly efficient thermal energy conversion through plasma-assisted combustion [1], [2]. There are many benefits to applying electromagnetic energy to a combustion reaction, including faster and more intense chemical energy conversion, increased flame stability over a broad range of conditions, reduction of pollution, improved fuel efficiency, and more reliable and rapid ignition [3]–[8]. Plasma-assisted combustion is particularly well suited for use in challenging conditions, as present in hypersonic flight, where complete and stable combustion is exceedingly difficult using traditional methods [6], [7].

Manuscript received March 17, 2011; revised May 8, 2011; accepted June 10, 2011. Date of publication August 22, 2011; date of current version December 14, 2011. This work was supported by AFOSR under Award FA9550-09-1-0282 and Award FA9550-10-1-0556) with Dr. J. Tishkoff as Technical Monitor.

S. Hammack, X. Rao, and T. Lee are with Michigan State University, East Lansing, MI 48824 USA (e-mail: hammacks@msu.edu).

C. Carter is with the Air Force Research Laboratory, Wright-Patterson AFB, OH 45433 USA.

Color versions of one or more of the figures in this paper are available online at http://ieeexplore.ieee.org.

Digital Object Identifier 10.1109/TPS.2011.2161778

While the enhancement of a flame using electromagnetic energy has been well studied and quantified, the exact mechanism(s) responsible for enhancement are still actively being explored. A number of studies have provided a glimpse into various aspects of this process [9]–[14]. Flame enhancement is likely a product of multiple physical and chemical plasma-flame interactions, including the following: 1) decomposition of the fuel from larger to smaller hydrocarbons and creation of radicals via collision with electrons; 2) radiation-induced electron excitation; 3) increased flame temperature by ohmic heating; 4) production of excited state species, ions, and electrons; and 5) *in situ* fuel reformation. To date, a large number of different discharge systems including microwave, dc, and radio frequency (RF) have been investigated by various research groups [4], [15]–[22], [24] using both experimental and numerical approaches. Nonetheless, the prospect of gaining insight into the synergistic integration of electrodynamics and combustion chemistry is a formidable challenge and requires further work. An extensive review can be found in [1].

The efficiency of a plasma-assisted combustion system, as a measure of the value of energetic enhancements versus its energy use, is critical in the assessment of such a system for practical implementations. In previous work, we have investigated the use of a highly efficient *direct coupling* method, where a plasma is generated spatially coincident with the flame reaction zone [23], enabling plasma-induced flame enhancement at very low power levels. The plasma and flame complement each other, as elevated temperature and reactivity of the plasma discharge initiate and enhance combustion, and the free electrons and heat release in the flame lower the power needed to sustain the plasma and increase the level of ionization. This study furthers the demonstration and understanding of direct coupling by extending its application to more realistic flame geometries and higher combustion powers. The study analyzes the physicochemical effects of direct coupling through imaging of spatially resolved hydroxyl (OH) concentrations and temperature fields using planar laser-induced fluorescence (PLIF) and Rayleigh scattering, respectively.

II. Experimental Setup

A. Microwave Waveguide Plasma Applicator

A novel microwave waveguide plasma system has been developed in collaboration with "Amarante Technologies" to directly couple microwave energy into flames with various geometries. The plasma system allows for complete access of the plasma-enhanced flame for laser and optical diagnostics

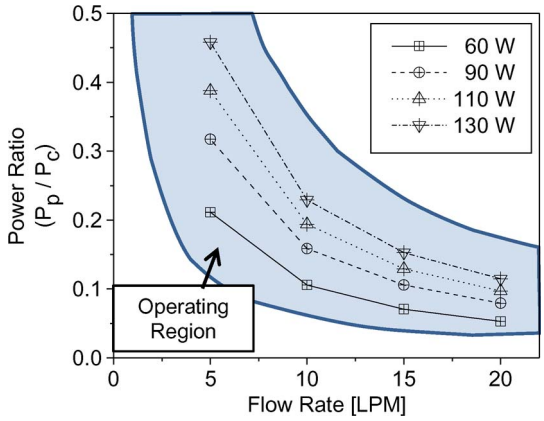

Fig. 1. Plot of the plasma-to-combustion-power ratio the torch operates at. The shaded region shows the total operable region. Flow rate is the total flow rate for a stoichiometric premixed methane/air flame.

at combustion power levels up to about 1 kW. Microwave radiation can be generated in excess of 1 kW but also as low as 30 W. Fig. 1 shows a plot of operating power ratios expressed as the absorbed plasma power to combustion power, ranging from 5% to 50% for the various conditions.

Fig. 2 (top) shows a schematic diagram of the microwave plasma discharge system. The microwave energy is generated by a research-grade 2.45-GHz magnetron directly mounted to a WR284 waveguide and powered by an SM840 power supply. The microwave transmission inside the WR284 waveguide is in TE_{10} mode. A directional coupler is mounted next to the magnetron head and is used to measure the incident power. A circulator is used to direct reflected energy into a dummy load with a coupler, so that reflected energy can also be measured. Both the magnetron and dummy load are water cooled. The three-stub tuner and sliding short are used to adjust the electric field and impedance to match the load of the plasma applicator and the nozzle. The plasma applicator is a nozzle allowing for direct coupling of plasma and flame.

Fig. 2 (bottom) illustrates the plasma applicator and nozzle, which also acts as the torch for combustion. The nozzle has a solid electrode that protrudes inside the WR284 waveguide. Microwave energy travels through the nozzle, acting as a coaxial guide, in transverse electromagnetic mode. The internal geometry of the nozzle is specially optimized for plasma ignition by delivering a high electric field at the nozzle tip. A plasma discharge is initiated by adjusting the standing wave's maximum E-field position inside the waveguide using the sliding short. As the standing wave moves inside the waveguide, the E-field at the nozzle tip also varies. When the E-field reaches the breakdown threshold, air around the electrode tip will be ionized, generating a plasma discharge that sits entirely above the surface of the nozzle and is accessible to direct optical measurements. To aid in the design of the nozzle, the electric field was calculated numerically from Maxwell's equations using the "RF Electromagnetic Solver" module of the program COMSOL MultiPhysics 3.4. For this simulation, the medium is air, and all boundaries are assumed to be perfect conductors.

This system can be compared to other modern microwave devices in the field. Some systems use an internal torch, inside

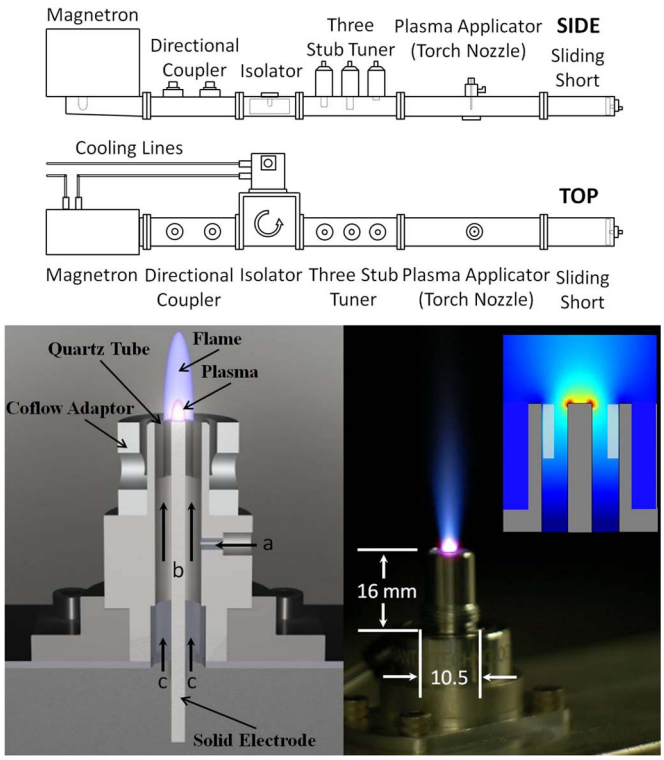

Fig. 2. (Top) Diagram of the microwave plasma waveguide system. (Bottom left) Diagram of the plasma applicator nozzle. (Bottom right) Plasma-coupled methane/air premixed flame. (Inset bottom right) Electric field solution from COMSOL MultiPhysics RF Electromagnetic Solver.

the waveguide itself, where the flame is held in a location of high electric field to observe subcritical microwave combustion enhancement [21]. Other devices use a coaxial design with differing electrode lengths to improve the efficiency of the field transition to a surface wave [24]. In many cases, a pulsed source is utilized to improve energetic efficiency. These constructions serve to maximize efficiency but can complicate diagnostics due to restricted optical access to the discharge and/or flame.

This system has been developed to produce a direct-coupled plasma-enhanced flame accessible to optical and laser diagnostics. The torch would likely be more efficient with a truncated inner electrode, where the outer electrode (nozzle body) extended further than the inner solid electrode; however, a heavy interest in complete access to the plasma ignition and coupling point directed the decision to use a "flush" configuration, where the electrodes end at the same length. Simulation work to improve the system geometry will continue, including the use of improved concurrent electromagnetic particle-in-cell (ICEPIC) code, which has recently been used to model this geometry, generating an argon plasma as a preliminary study.

B. Torch Geometry

The torch nozzle allows for gas flow into the plasma discharge. To produce a premixed flame, a mixture of fuel and air enters into the side of the aluminum nozzle through (a) inlet and exits into the plasma discharge at the tip of the (b) electrode. A Teflon insert prevents the flow from entering into the microwave cavity at the bottom off the nozzle while allowing

microwave energy to travel upward (c). This configuration produces a direct-coupled plasma-assisted combustion (PAC) discharge. A coflow adaptor allows for an annular stream of gas around the nozzle but was not needed here. In data presented here, the reactants are methane and air.

C. Laser Diagnostics

The excitation of OH was made using the $Q_1(8)$ transition from the $A^2\Sigma^+ - X^2\Pi$ (1,0) [25] band, which requires narrowband UV light near 283 nm. The measurements were conducted using a dye laser (Lumonics Hyperdye HD-300) with an output of 7-ns pulses at 566 nm, which was subsequently frequency doubled through an Inrad Autotracker (ATIII) to a final frequency of 283 nm. The laser is pulsed at 10 Hz and has a spectral line width of about 0.1 cm^{-1} at 283 nm. The pulse energy was recorded digitally using a fast photodiode and an oscilloscope and attenuated to ensure operation within the linear fluorescence regime. The laser was expanded into a sheet, and the fluorescence signal was collected at 90° using an intensified charge-coupled device (CCD) camera (Roper Scientific Superblue PIMAX) fitted with a Cerco 45-mm-focal-length f/1.8 lens, and a high-transmission ($> 80\%$ at 310 nm) bandpass filter (Custom fabrication—Laser Components GmbH). A flat flame burner was used for calibration of the laser wavelength, and a Hencken burner was used to correlate the signal intensity with the OH number density using previously performed absorption measurements.

Rayleigh scattering thermometry [26] was conducted using the frequency-doubled output of an Nd:YAG laser ($\lambda = 532$ nm). Scattering measurements were used here, rather than other thermometry methods that are based on assumptions of the population of quantum states, due to the nonequilibrium nature of the plasma discharge. Scattering was collected through a bandpass filter centered at 532 nm with a 10-nm full-width at half-maximum using a second intensified CCD camera (Roper Scientific Gen III PIMAX) fitted with a Nikon 58-mm-focal-length f/1.2 Noct-Nikkor lens. Black curtains enclosed the test section to limit background scattering, and sufficient signal quality was achieved, so that filtered Rayleigh scattering approaches were not required. The collected scattering is a measure of number density, from which a planar temperature profile can be obtained by utilizing the Ideal Gas Law. By normalizing the images by an image of Rayleigh scattering in air with no discharge, the laser intensity is eliminated from the calculation. The temperature is given by

$$T_d = \frac{\sigma_d I_a}{\sigma_a I_d} T_a \tag{1}$$

where σ_d and σ_a are the Rayleigh scattering cross sections of the discharge gas and air, respectively. I_a is the reference scattering intensity in air at temperature T_a, and I_d is the scattering intensity from the plasma discharge. For combustion cases, gas composition in the reaction zones was assumed to be the stoichiometric products of methane/air, which limits error due to composition assumptions to less than 10%, as nitrogen is still the primary constituent. For air plasmas, composition of dry air was used for the cross sections. To reduce Mie scattering, air and reactant flows were filtered, the camera was positioned to collect backscattering, and averaged images were calculated as the median of 200 images.

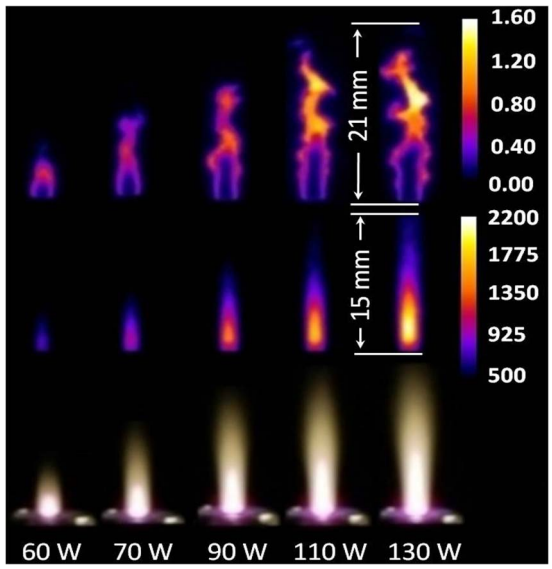

Fig. 3. Images of (top) OH number density [10^{16} cm^{-3}], (middle) averaged temperature (in degrees Kelvin), and (bottom) discharge of an air plasma discharge for varying microwave power levels, increasing left to right (15-l/min flow rate).

III. Results and Discussion

A. Air-Only Plasma Discharge

Imaging results are shown in Fig. 3 as a function of increasing microwave power for just the plasma discharge in air without combustion. All images and photographs are at a flow rate of 15 l/min. The first row contains instantaneous OH number density images, the second row contains the median temperature images, and the third row contains photographs of the discharge at an exposure of 10 ms. The microwave power level is simply the difference between incident and reflected microwave values from the waveguide. The magnetron output was fixed at its lowest possible value, i.e., 360 W; for all discharges, the effective power input into the plasma was adjusted by manipulating the reflected power through tuning. Percent power reflected will then be the difference between the magnetron power (360 W) and reported microwave power divided by the magnetron power. A microwave power level ranging from 60 to 150 W corresponds to ∼83%–58%. The waveguide can be tuned to reflect very little power (10%).

Observation of the image series clearly illustrates an increase in discharge volume and emission, OH number density, and temperature as microwave power increases. Temperature in the air plasma is quite high with a highly focused power deposition. OH production due to the plasma discharge comes solely from the water vapor in the ambient air, reaching densities up to 10^{16} cm^{-3} in a laboratory with moderate humidity (40%–50% relative humidity). This is demonstrated clearly in the OH PLIF images as the center plasma discharge volume is devoid of OH radicals because this is dry compressed air. Instead, the area above the discharge, where ambient air can mix with the hot

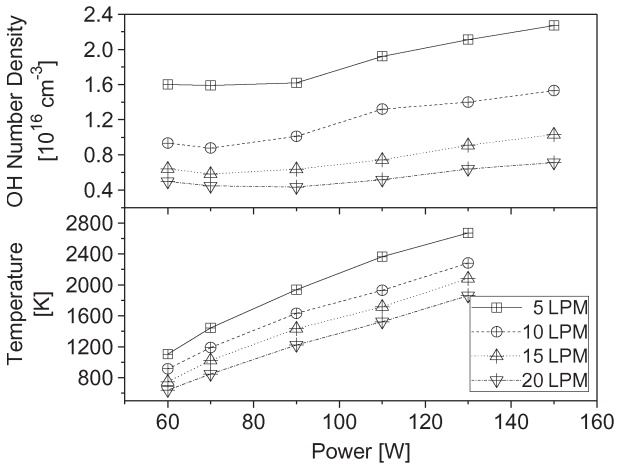

Fig. 4. (Top) OH number density and (bottom) temperature versus power in the air plasma discharge for varying flow rates.

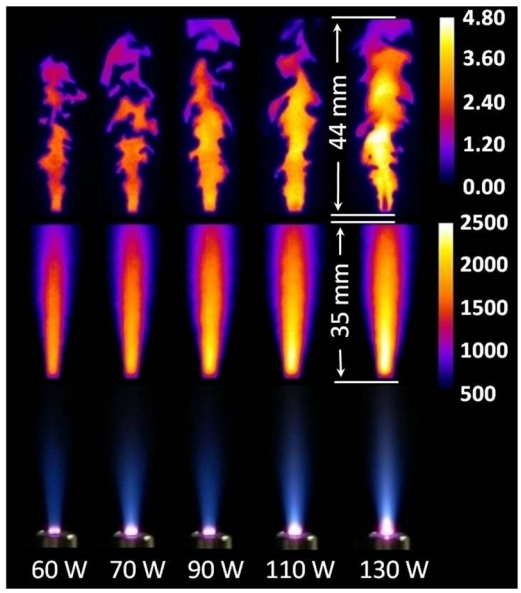

Fig. 5. Images of (top) OH number density [10^{16} cm^{-3}], (middle) averaged temperature (in degrees Kelvin), and (bottom) plasma-coupled combustion discharge at varying microwave power levels, increasing left to right. The total flow rate is 15 l/min at an equivalence ratio of $\phi = 1$.

discharge, contains an amount of OH usually associated with levels found in methane/air combustion [8]. It should be noted that OH populations in the Boltzmann fraction are considered to be constant, which is an adequate assumption for a temperature range of about 1050–2600 K ($< 10\%$). However, additional error is expected at lower temperature regions below 800 K and above 3000 K, where an underprediction of OH occurs. No adjustment has been made due to lack of simultaneous temperature–OH-density data in the turbulent flow field. The bright air discharge in the photographs indicates emissions from all visible wavelengths typically found in this type of plasma (mainly emissions from OH, N_2, N_2^*) [27]. The discharge is estimated to be weakly ionized with an electron density of about 10^{11}–10^{12} cm^{-3} with an estimated e-field on the order of the breakdown threshold of air, i.e., 10^6 V/m.

Fig. 4 shows the plotted relationship between OH number density, temperature, and power. Here, the OH number density is defined as the maximum value in an averaged image and calculated as the mean value of each pixel from 200 single images. With no hydrogen source on the dry air flow, there is a lack of radical concentration in the plasma volume. The OH production observed is a product of the water vapor in the ambient air reacting with free electrons produced in the plasma, as well as atomic oxygen. The mechanisms of interests are $e + H_2O \rightarrow e + H + OH$ [28] and $H_2O + O(^1D) \rightarrow 2OH$ [29].

The OH number density remains relatively stable over a power range of 60–90 W. Changes in power level do not significantly affect the OH production chemical pathways. At higher powers, the OH number density increases near-linearly with power. The OH number density is inversely related to flow rate. This is expected, as a lower flow rate allows for greater power deposition into a given volume of air above the torch. Once again, underprediction of OH concentrations is expected at very low and very high temperature regions, for which no correction has been made.

Temperature increases as a function of power in a near-linear manner. Like OH number density, the temperature is inversely related to flow rate because of the greater power density at lower flow, which, in turn, will increase the production of OH radicals from water vapor in the ambient air. The plotted temperature data are the mean values of a high-temperature region in the averaged temperature profiles, which are calculated as the median of 200 single images. The region was defined as a 0.75-mm $\times$ 1-mm area, where the mean temperature was greatest. Temperatures range from about 650 K at 60 W and 20 l/min, to 2650 K at 130 W and 5 l/min.

B. Plasma-Assisted Combustion

OH number density, temperature, and photographs of a premixed plasma-assisted combustion case are shown in Fig. 5. For all conditions, the flow rates are significantly fast (a minimum of about 5 m/s) that a flame cannot be naturally stabilized but must be "anchored" by the plasma discharge. The same trends observed in the air-only discharge can be seen in the combustion case; discharge volume, emission, OH number density, and temperature all increase with increasing microwave power. OH number density is significantly higher than in the air discharge due to additional hydrogen atoms available from the hydrocarbon combustion chemistry. The discharge temperature is greater than in the air-only case, and the high temperature region is much larger due to the overlap with the expanding flame volume. The photographs show a violet plasma discharge, indicating strong emission in the UV range. The flame emits a blue hue, typical of CH^* emission in premixed combustion, accompanied by heat release and increased radical concentration, indicating ignition. Spectrally resolved chemiluminescence of the coupled discharge strongly agrees with that of a flame, confirming combustion.

OH number density and temperature in the premixed discharge are plotted for a range of absorbed power in Fig. 6. OH number density for different flow rates remains relatively constant, even though the energy per molecule is greater as the flow is reduced. In comparing the OH number density,

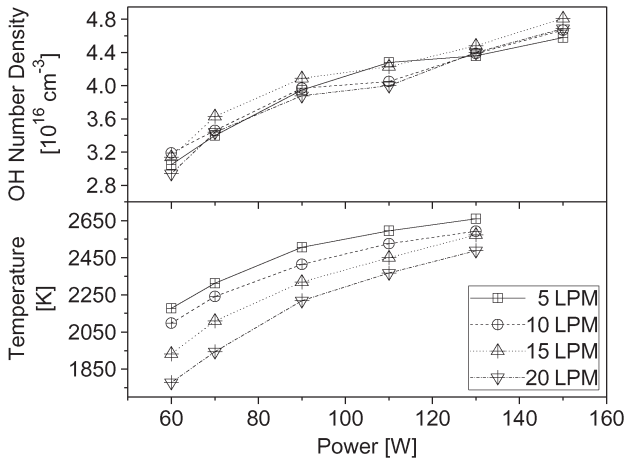

Fig. 6. (Top) OH number density and (bottom) temperature versus power in the premix plasma discharge for varying flow rates. Equivalence ratio is $\phi = 1$.

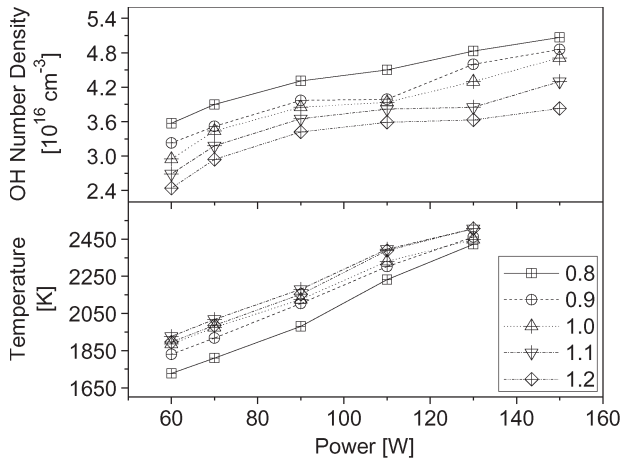

Fig. 7. (Top) OH number density and (bottom) temperature versus power in the premixed plasma discharge for varying equivalence ratios. The total flow rate is 15 l/min.

temperature, and photographic images for different flow rates at constant power, it is observed that the reaction volume is greater as the flow is lowered, due to the lower momentum of the gas flow, resulting in a dilution of OH radicals. We conclude that the increasing energy per molecule and dilution effects are similar in magnitude, effectively canceling each other. Unlike the air-only discharge, OH number density increases over the entire power range.

In analyzing temperature, we can see that, at lower powers and higher flow rates, the temperature (median of 200 single-shot images) is below the adiabatic temperature of the flame ($>$ 2200 K for methane/air). This is likely due to incomplete combustion caused by the higher flow velocities, although it is important to note that, as median values, these temperatures are not the absolute maximum for a single image. In addition, it should be noted that, for a given flow rate, unlike the air plasma discharge, the increase in temperature as a function of power is relatively small. There appears to be an asymptotic limit to temperature, approached by all flow rate lines, where the combustion becomes fully complete. This leads us to speculate that, while, in the air plasma, most of the plasma energy is transferred to the gas as heat, other transfer channels play a significant role when the plasma energy is coupled into a premixed flame where electrons and ions are already present.

Fig. 7 shows the observed OH number density and temperature as a function of power for various equivalence ratios. Temperature is highest at rich conditions due to greater chemical heat release, whereas OH number density is maximized in lean conditions due to the abundance of oxygen atoms. Both temperature and OH density increase with an increase in power.

C. Power Into Heating

Analysis of gas temperature near the plasma discharge was conducted to investigate the thermal nature of the discharge. The heating of the gas flow can be calculated from the increase in temperature as power increases and expressed as a heating power using the following:

$$P = \dot{V} c_p \rho \Delta T \tag{2}$$

TABLE I
PLASMA HEATING IN AN AIR DISCHARGE AND PLASMA-ASSISTED COMBUSTION

MW Power Interval [W]	ΔT [K]		Heating [W]		Heating [% of ΔP]	
	Air	CH4/Air	Air	CH4/Air	Air	CH4/Air
60 to 70	134.24	83.05	6.92	1.63	69.2%	16.3%
70 to 90	258.71	180.35	10.52	3.47	52.6%	17.3%
90 to 110	216.26	86.48	7.09	1.64	35.4%	8.2%
110 to 130	170.57	59.72	4.83	1.14	24.2%	5.7%

where $\dot{V}$ is the volumetric flow rate, c_p is the specific heat, ρ is the density, and ΔT is the change in mean discharge temperature weighted for the 3-D geometry. The gas heating can be expressed as a percentage of an increase in microwave power, where ΔT is evaluated between the two power levels.

Table I contains the increase in temperature, heating power, and heating as a percent of the increase in microwave power for both an air-only discharge and plasma-assisted combustion. The percent power into heating is much higher in the air-only discharge than in the PAC discharge, where a very large portion of plasma energy couples as nonthermal effects. As power is increased, the expression of plasma energy as heat decreases. From this data, it is demonstrated that the thermal effects are lesser in a plasma-enhanced flame than in air and lesser at greater microwave powers. The power into heating the air plasma is about four times greater than for PAC over the same power interval. At these conditions, the microwave energy per molecule is highest, and nonthermal effects, including fuel breakdown through electron impact dissociation and excited state species interaction, are maximized in relation to heating interactions, such as relaxation and energy transfer. This introduces the need to assess the value in using greater plasma energy to increase nonthermal effects. Future simulation studies utilizing ICEPIC code will focus on examining these trends.

IV. Conclusion

A microwave cavity with an external plasma applicator nozzle has been used to demonstrate plasma-assisted combustion by direct coupling. Electromagnetic energy from a continuous-source 2.45-GHz magnetron has been focused to a nozzle tip, producing a plasma discharge, where it initiates and stabilizes a flame. The plasma-coupled flame has been analyzed using hydroxyl radical PLIF and Rayleigh scattering thermometry to measure OH number density and temperature.

Increases in both OH number density (up to 50 percent) and temperature (up to 40%) in a plasma-enhanced methane/air flame have been observed over a power range of 60–150 W or 5%–50% of the combustion power, depending on flow conditions. For a given power increase, the flame has been heated much less than an air-only plasma discharge, as a greater portion of plasma energy was expressed through nonthermal effects, particularly at high-energy-per-molecule conditions. Further studies into plasma-discharge-coupled numerical simulations would further elucidate the complex interaction between the plasma and flame chemistry.

References

[1] S. M. Starikovskaia, "Plasma assisted ignition and combustion," *J. Phys. D, Appl. Phys.*, vol. 39, no. 16, pp. R265–R299, Aug. 2006.

[2] A. Y. Starikovskii, "Plasma supported combustion," *Proc. Combustion Inst.*, vol. 30, no. 2, pp. 2405–2417, Jan. 2005.

[3] L. Bromberg, D. R. Cohn, A. Rabinovitch, and J. Heywood, "Emissions reductions using hydrogen from plasmatron fuel converters," *Int. J. Hydrogen Energy*, vol. 26, no. 10, pp. 1115–1121, Oct. 2001.

[4] W. Kim, H. Do, M. G. Mungal, and M. A. Cappelli, "Plasma-discharge stabilization of jet diffusion flames," *IEEE Trans. Plasma Sci.*, vol. 34, no. 6, pp. 2545–2551, Dec. 2006.

[5] D. H. Lee, K. T. Kim, M. S. Cha, and Y. H. Song, "Optimization scheme of a rotating gliding arc reactor for partial oxidation of methane," *Proc. Combustion Inst.*, vol. 31, no. 2, pp. 3343–3351, Jan. 2007.

[6] A. B. Leonov, D. A. Yarantsev, A. P. Napartovich, and I. V. Kochetov, "Plasma-assisted ignition and flameholding in high-speed flow," presented at the 44th AIAA Aerospace Sciences Meeting, Reno, NV, 2006, AIAA-2006-563.

[7] S. B. Leonov and D. A. Yarantsev, "Plasma-induced ignition and plasma-assisted combustion in high-speed flow," *Plasma Sources Sci. Technol.*, vol. 16, no. 1, pp. 132–138, Feb. 2007.

[8] T. Ombrello, X. Qin, Y. Ju, A. Gutsol, A. Fridman, and C. Carter, "Combustion enhancement via stabilized piecewise nonequilibrium gliding arc plasma discharge," *AIAA J.*, vol. 44, no. 1, pp. 142–150, Jan. 2006.

[9] W. Kim, M. M. Godfrey, and M. A. Cappelli, "The role of *in situ* reforming in plasma enhanced ultra lean premixed methane/air flames," *Combustion Flame*, vol. 157, no. 2, pp. 374–383, Feb. 2010, DOI:10.1016/j.combustflame.2009.1006.1016.

[10] E. Mintusov, A. Serdyuchenko, I. Choi, W. R. Lempert, and I. V. Adamovich, "Mechanism of plasma assisted oxidation and ignition of ethylene-air flows by a repetitively pulsed nanosecond discharge," presented at the 46th AIAA Aerospace Sciences Meeting Exhibit, Reno, NV, 2008, AIAA 2008-1106.

[11] T. Ombrello, J. Yiguang, and F. Alexander, "Kinetic ignition enhancement of diffusion flames by nonequilibrium magnetic gliding arc plasma," *AIAA J.*, vol. 46, no. 10, pp. 2424–2433, Oct. 2008.

[12] O. Timothy, W. S. Hee, and J. Yiguang, "Lifted flame speed enhancement by plasma excitation of oxygen," presented at the 47th AIAA Aerospace Sciences Meeting Exhibit, Reno, NV, 2009, AIAA-2009-689.

[13] W. Sun, M. Uddi, T. Ombrello, S. Won, C. Carter, and Y. Ju, "Effects of non-equilibrium plasma discharge on counterflow diffusion flame extinction," *Proc. Combustion Inst.*, vol. 33, no. 2, pp. 3211–3218, 2011.

[14] M. Uddi, N. Jiang, E. Mintusov, I. V. Adamovich, and W. R. Lempert, "Atomic oxygen measurements in air and air/fuel nanosecond pulse discharges by two photon laser induced fluorescence," presented at the 46th AIAA Aerospace Sciences Meeting Exhibit, Orlando, Fl, 2008, AIAA 2008-1110.

[15] L. Bromberg, D. R. Cohn, A. Rabinovitch, and J. Heywood, "Emissions reductions using hydrogen from plasmatron fuel coverters," *Int. J. Hydrogen Energy*, vol. 26, no. 10, pp. 1115–1121, Oct. 2001.

[16] N. Chintala, A. Bao, G. Lou, and I. V. Adamovich, "Measurements of combustion efficiency in nonequilibrium RF plasma-ignited flows," *Combustion Flame*, vol. 144, no. 4, pp. 744–756, Mar. 2006.

[17] Y. D. Korolev and I. B. Matveev, "Nonsteady-state processes in a plasma pilot for ignition and flame control," *IEEE Trans. Plasma Sci.*, vol. 34, no. 6, pp. 2507–2513, Dec. 2006.

[18] I. V. Kuznetsova, N. Y. Kalashnikov, A. F. Gutsol, A. F. Fridman, and L. A. Kennedy, "Effect of 'overshooting' in the transitional regimes of the low-current gliding arc discharge," *J. Appl. Phys.*, vol. 92, no. 8, pp. 4231–4237, Oct. 2002.

[19] G. Lou, A. Bao, M. Nishihara, S. Keshav, Y. G. Utkin, J. W. Rich, W. R. Lempert, and I. V. Adamovich, "Ignition of premixed hydrocarbon–air flows by repetitively pulsed, nanosecond pulse duration plasma," *Proc. Combustion Inst.*, vol. 31, no. 2, pp. 3327–3334, Jan. 2007.

[20] A. Y. Starikovskii, N. B. Anikin, I. N. Kosarev, E. I. Mintoussov, M. M. Nudnova, A. E. Rakitin, D. V. Roupassov, S. M Starikovskaia, and V. P. Zhukov, "Nanosecond-pulsed discharge for plasma-assisted combustion and aerodynamics," *J. Propulsion Power*, vol. 24, no. 6, pp. 1182–1197, 2008.

[21] E. S. Stockman, S. H. Zaidi, R. B. Miles, C. D. Carter, and M. D. Ryan, "Measurements of combustion properties in a microwave enhanced flame," *Combustion Flame*, vol. 156, no. 7, pp. 1453–1461, Jul. 2009.

[22] S. H. Zaidi, E. Stockman, X. Qin, Z. Zhao, S. Macheret, Y. Ju, R. B. Miles, D. J. Sullivan, and J. F. Kline, "Measurements of hydrocarbon flame speed enhancement in high-Q microwave cavity," presented at the 44th AIAA Aerospace Sciences Meeting Exhibit, Reno, NV, 2006, AIAA-2006-1217.

[23] X. Rao, K. Hemawan, I. Wichman, C. Carter, T. Grotjohn, J. Asmussen, and T. Lee, "Combustion dynamics for energetically enhanced flames using direct microwave energy coupling," *Proc. Combustion Inst.*, vol. 33, no. 2, pp. 3233–3240, 2011, DOI:10.1016/j.proci.2010.06.024.

[24] A. M. Davydov, S. I. Gritsinin, I. A. Kossyi, Y. M. Shikhman, and V. A. Vinogradov, "Application of MW plasma generator for ignition of kerosene/air mixture," *IEEE Trans. Plasma Sci.*, vol. 36, no. 6, pp. 2909–2917, Dec. 2008.

[25] K. Kohse-Hoinghaus and J. B. Jeffries, *Applied Combustion Diagnostics*. New York: Taylor & Francis, 2002.

[26] R. Miles, W. Lempert, and J. Forkey, "Laser Rayleigh scattering," *Meas. Sci. Technol.*, vol. 12, no. 5, pp. R33–R51, May 2001.

[27] M. Laroussi, X. Lu, and C. Malott, "A non-equilibrium diffuse discharge in atmospheric pressure air," *Plasma Sources Sci. Technol.*, vol. 12, no. 1, pp. 53–56, Feb. 2003.

[28] R. Ono and T. Oda, "Dynamics of ozone and OH radicals generated by pulsed corona discharge in hu mid-air flow reactor measured by laser spectroscopy," *J. Appl. Phys.*, vol. 93, no. 10, pp. 5876–5882, May 2003.

[29] B. Benstaali, P. Boubert, B. Cheron, A. Addou, and J. Brisset, "Density and rotational temperature measurements of the OH and NO radicals produced by a gliding arc in humid air," *Plasma Chem. Plasma Process*, vol. 22, no. 4, pp. 553–571, Dec. 2002.

Stephen Hammack (S'11) was born in Chicago, IL, on May 13, 1988. He received the B.S. degree in mechanical engineering, in 2009, from Michigan State University, East Lansing, where he is currently working toward the Ph.D. degree.

He is currently a Graduate Research Assistant with Michigan State University. His research interests include laser diagnostics of combustion and plasma-assisted combustion.

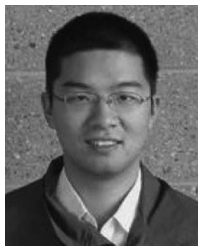

Xing Rao was born in Jinxi, China, on March 26, 1985. He received the B.S. degree in mechanical engineering and the M.S. degree in nuclear engineering from Tsinghua University, Beijing, China, in 2005 and 2007, respectively, and the Ph.D. degree in mechanical engineering from Michigan State University, East Lansing, in 2010.

He is currently a Particle Accelerator Mechanical Engineer with the Facility for Rare Isotope Beams, Michigan State University

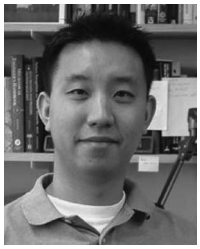

Tonghun Lee was born in Seoul, Korea, on April 3, 1974. He received the B.S. degree in mechanical engineering from Yonsei University, Seoul, in 2000, and the M.S. and Ph.D. degrees in mechanical engineering from Stanford University, Stanford, CA, in 2002 and 2006, respectively.

He is currently an Assistant Professor with the Department of Mechanical Engineering, Michigan State University, East Lansing. His research group at Michigan State University is devoted to fundamental research in applying laser-based optical methods for development of advanced combustion and propulsion system technologies. His research interests include laser diagnostics of high-pressure combustion systems, plasma-enhanced flames, and oxidation of novel biofuels.

Campbell Carter was born in Refugio, TX, in 1958. He received the B.S. degree from the University of Texas, Austin, and the Ph.D. degree from Purdue University, West Lafayette, IN, both in mechanical engineering.

Upon leaving Purdue University, he joined the Combustion Research Facility, Sandia National Laboratories, as a Postdoctoral Fellow, where he worked with Dr. R. Barlow on making simultaneous measurements of major and minor combustion species in turbulent flames. He joined Systems Research Laboratories in 1993 and then Innovative Scientific Solutions, Inc, in 1997, developing and applying laser diagnostic techniques for the advanced propulsion group at the U.S. Air Force Research Laboratory (AFRL), Wright-Patterson AFB, OH. Since 2002, he has been with AFRL. His research interests include the development and application of advanced laser diagnostics of complex reactive flows.